A New 6-DOF Haptic Device for Teleoperation of 6-DOF Serial Robots

Minh Hung Vu and Uhn Joo Na

***Abstract*—A new 6-DOF parallel haptic device is developed and presented in this paper. The haptic device consists of two 3-DOF parallel structures connected with a steering handle. The design satisfies requirements of low inertia, quick motion, large orientation angles, and large applied torques. Kinematics for position and differential motion is analyzed for the 6-DOF haptic device. Static force relation between the user force and motor torque is also analyzed and implemented on the controller. The control system for the teleoperation of 6-DOF serial robot is developed. The closed loop impedance force control system is analyzed and realized on the digital controller. Tele-operation of a 6-DOF serial robot using this haptic device is demonstrated. Experiments show that dynamic forces caused by the haptic device are well compensated with the closed loop force control.**

***Index Terms*—Force control, haptic control, haptic device, haptic interface, master-slave control, telerobotics, tele-operation.**

NOMENCLATURE

F_c	Torque/force vector to generate motion of handle
F_e	Contacting torque/force vector from environment
F_f	Torque/force vector from user's hand
$K_h(s)$	Haptic force controller
$K_r(s)$	Robot position controller
L	Force transformation matrix between upper and lower end effectors to center of steering handle
x_h	Position and orientation vector of haptic device
x_r	Position and orientation vector of robot
Z_e	Environment model
$\hat{Z}_h$	Haptic device dynamics
Z_r	Robot dynamics
Z_u	User's hand model
τ_c	Joint torque vector of haptic device
τ_h	Total torque vector of haptic device motors
τ_m	Torque of haptic device motors from control output
τ_u	Torque of haptic device motors from user's hand
τ_t	Joint torque vector of upper structure
τ_b	Joint torque vector of lower structure
θ_h	Active joint angle vector of haptic device
θ_r	Joint angle vector of robot

Manuscript received November 19, 2010; revised May 13, 2011; accepted July 9, 2011. Date of publication September 19, 2011; date of current version November 9, 2011. This work was supported by Kyungnam University Research Fund. The Associate Editor coordinating the review process for this paper was Dr. Atif Alamri.

The authors are with the School of Mechanical Engineering and Automation, Kyungnam University, Masan 630-701, Korea (e-mail: uhnjoona@kyungnam.ac.kr).

Color versions of one or more of the figures in this paper are available online at http://ieeexplore.ieee.org.

Digital Object Identifier 10.1109/TIM.2011.2164285

I. INTRODUCTION

HAPTIC INTERFACES have become active research area since the computing power of the processors has increased rapidly. Haptics applications such as games, multimedia, computer interaction, education and training, and teleoperation require a particular haptic device structure for various purposes. For example, art graphics on computer requires an accurate haptic device but small feedback forces, while 4-D-film simulators do not require accurate haptic devices but large feedback forces.

Typically the mechanism of haptic devices is divided into serial structures and parallel structures. Serial haptic devices such as PHANToM Premium, PHANToM OMNI and VIRTUOSE 6D [1]–[3] have open kinematic structures such that they usually provide a large workspace but show lack of strength and compactness, while parallel haptic devices have closed kinematic structures such that they provide a smaller workspace but show strength and precision. The workspace, maximum force/torque and resolution of position for a specific application should be considered in design of haptic devices [4], [5].

The 6-DOF parallel haptic devices are often composed of three or six legs. Six-legged 6-DOF parallel structures provide high strength, compactness and precision but their workspace and orientation are small [6]. Three-legged 6-DOF parallel structures provide simple and light interfaces. Their orientation and workspace are improved since each leg often consists of at least two links. However, the resolution and precision of movements as well as strength are reduced [7]–[9].

Parallel haptic devices with legs and a moving platform typically provide small orientation due to the kinematic constraints between legs and a moving platform. Workspace of orientation for parallel haptic devices can be improved when the moving platform is replaced with a handle (or stylus). All legs are then divided into two groups connected to each end of the handle. Lee *et al.* [10] proposed a new 5-DOF haptic device which has five legs connected with a stylus. Each leg is controlled by a prismatic actuator to change its length. This design provides a light interface and large workspace. Stocco *et al.* [11] developed a 5-DOF haptic device which has four legs attached on two rotational moving frames. Two groups of legs are connected to each end of handle (or pen) through a universal joint. This haptic device provides three translations and two rotations. However, the change of orientation affects the position (coupling). This design has four motors on the moving frames so that it limits the size of motors and increases inertia effect of the device.

Teleoperation using a haptic device is emerging and attracting researchers [12]–[14]. Tele-operation is particularly useful to handle remote objects in hostile environments or in a special environment such as minimal invasive surgery. The teleoperation in the virtual environment is also useful for training before it is tested in the real environment. Gupta *et al.* [15] developed a real teleoperation system of anthropomorphic robotic arm with gripping force sensing using bilateral master-slave method. Typically there are four different master-slave systems such as position-position, position-force, force-position and force-force systems [16].

The position-force bilateral method is often used in teleoperation systems. The master devices generate motions for slave devices and receive feedback forces from the environments [17], [18]. Ando *et al.* [19] presented a full teleoperation control block in a real environment. Impedance force control and admittance force control are two force control techniques used for teleoperation of haptic devices. Impedance control is used for low friction and light structures [20] while admittance control is used for structures designed with gear systems [21]. Wen *et al.* [22] showed that the open loop impedance control produces 10% of force errors. The closed loop impedance control may improve the force performances. The full linear models of teleoperation system including haptic impedance, environment impedance and user's hand impedance are introduced to analyze the stability and performance of the controllers [23].

Teleoperation of slave robots using haptic devices should satisfy two main objectives; position control of the slave robot and accurate force sensing from the environment. For the position control the haptic device should provide the real-time trajectory commands for the slave robot to tract. Workspace of the haptic device should be properly designed to cover that of the slave robot. Detecting accurate contacting forces from the environment may present a difficult design problem. The user should feel actual forces from the environment not those of the structure of the haptic device. This implies that the haptic device should have lowest possible inertia and frictions to reduce the undesired forces from haptic dynamics. The undesired dynamic forces from the haptic device may also be compensated with the closed loop force control.

This paper extends the preceding works of 6-DOF haptic device [24]. A new 6-DOF haptic device is designed based on the criteria of low inertia, large workspace with large orientation angles, big static forces, and high stiffness. This new design has some advantages over the preceding works of 5-DOF haptic pen [11]. Kinematics for position and differential motion is analyzed for the 6-DOF haptic device. Teleoperation of a 6-DOF serial robot using this new 6-DOF haptic device is presented. The closed loop impedance force control of haptic device including user's hand impedance is analyzed and realized on the digital controller.

II. New 6-DOF Haptic Device

A new 6-DOF haptic device is designed and shown in Fig. 1. The designed 6-DOF haptic device utilizes two 3-DOF parallel structures similar to the 3-DOF Delta structure [25]. Each 3-DOF structure is connected to each end of the handle to provide 5-DOF motions. The handle provides one more DOF of twist motion to make a 6-DOF haptic device. The test rig of the new haptic device is shown in Fig. 2. This haptic device has six legs controlled by six gearless DC motors fixed on the base frame. Each leg is made of hollow aluminum to meet the low weight requirement. Two weight balances are attached on the back extension of the two middle legs to minimize the effect of gravity. Each leg is composed of two links connected by two 2-DOF revolute ball bearing joints such that one revolute joint connects two links while the other revolute joint connects the link to the end effector.

These two 3-DOF parallel structures are divided into the upper structure and the lower structure. The end effectors of the

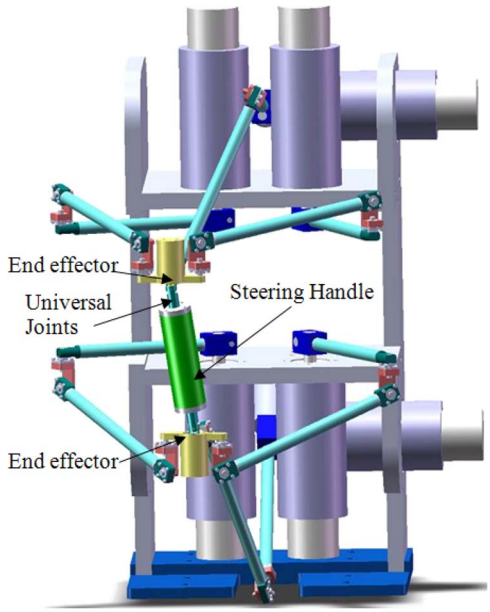

Fig. 1. New 6-DOF haptic device.

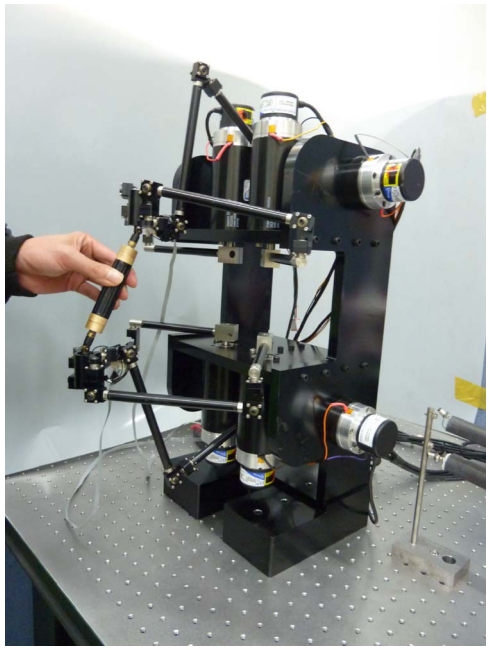

Fig. 2. Test rig of the new 6-DOF haptic device.

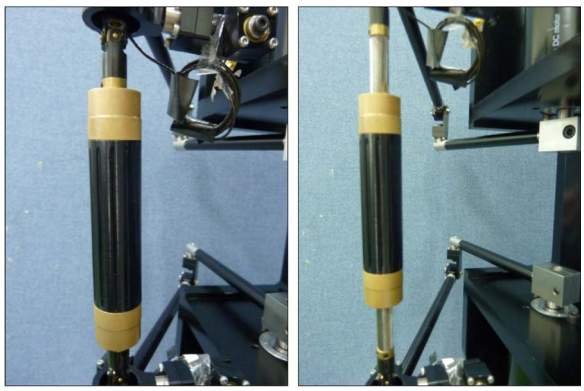

Fig. 3. Shortest length (left) and longest length (right) of steering handle.

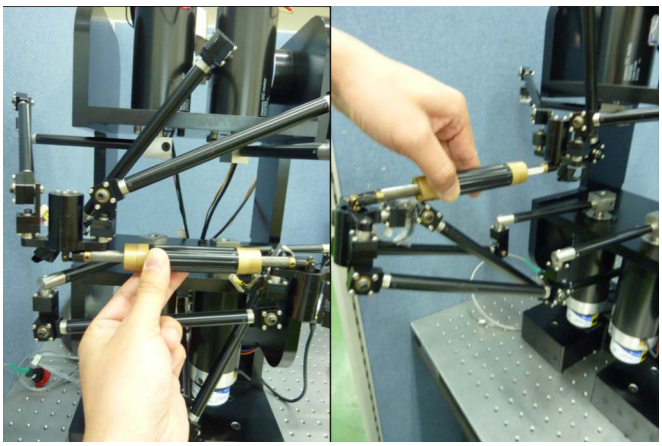

Fig. 4. Rotation about X-axis (left) and Y-axis (right).

upper and lower structures are connected to a steering handle via universal joints. Two 3-DOF force sensors are attached on the end effectors to measure the applied forces exerted by the user. The steering handle shown in Fig. 3 connects the upper and lower end effectors. The steering handle is designed to generate linear displacements when rotated, which gives the haptic device one more DOF of twist motion. The handle is assembled with the left and right lead screws so that the rotation of the handle leads to the linear movement of the screws at both ends.

Two universal joints are used to connect the lead screws to the upper and lower end effectors. The twisting rotation of the handle thus leads to the change of positions of the upper and lower end effectors. Fig. 3 shows that the handle can be extended linearly up to the limit (60 mm) for the 360° of rotation (γ).

The new haptic device provides large orientation angles to match up with the orientation workspace of the slave serial robot. The lengths of links are designed such that the haptic device may generate big enough rotations about three axes. The orientation angle α about X-axis and angle β about Y-axis in the handle fixed coordinate are demonstrated on the test rig in Fig. 4. The maximum angles of α and β are up to $\pm 90°$. The orientation and position of the center of the handle are completely decoupled so that maximum orientation angles may be realized while the position is kept.

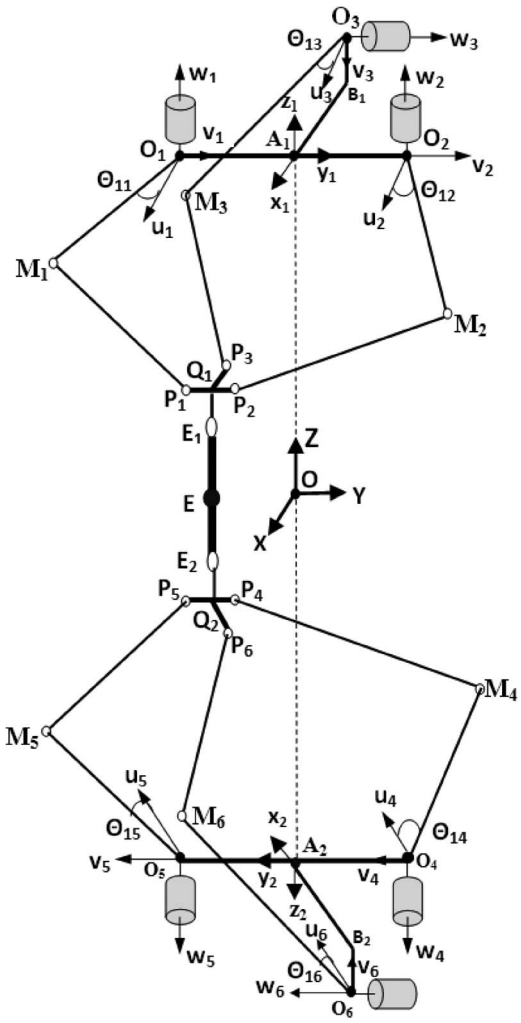

Fig. 5. Coordinate systems of the 6-DOF haptic device.

Since all six motors are fixed on the base frame, torque capacity of all motors can be freely selected while weights and inertias of the moving frame may be minimized. The designed haptic device can provide forces up to 30 N and torque up to 2 Nm. These are big enough values for the serial robot contacting with high stiffness environments.

III. Kinematic Analysis

A. Forward Kinematics

Forward kinematics is analyzed to determine the position and orientation of the center of the steering handle. Three different coordinate systems are used for forward kinematics; local leg coordinates $O_i u_i v_i w_i$, the upper base coordinate $A_1 x_1 y_1 z_1$ and the lower base coordinate $A_2 x_2 y_2 z_2$, and the global base coordinate $OXYZ$. The coordinate systems and dimensions of the 6-DOF haptic device are shown in Fig. 5 and Table I.

Joint angles of the leg 1 are defined on the local leg coordinate $(O_1 u_1 v_1 w_1)$ as shown in Fig. 6. Similarly joint angles of each leg, $\theta_{1i}\theta_{2i}$ and θ_{3i}, are defined on the local leg coordinates (motor coordinates) $O_i u_i v_i w_i$ to determine the local leg position vectors $\overrightarrow{O_i P_i}$. Joint angles θ_{1i} are measured from $O_i u_i$ axis

TABLE I
PARAMETER OF NEW 6-DOF HAPTIC DEVICE

Symbol	Description	Value
a	O_1A_1, O_2A_1, O_4A_2, O_5A_2	0.042 m
b	A_1B_1, A_2B_2	0.070 m
c	B_1O_3, B_2O_6	0.100 m
d	Q_1P_1, Q_1P_2, Q_1P_3, Q_2P_4, Q_2P_5, Q_2P_6	0.030 m
h	Q_1E_1, Q_2E_2	0.020 m
l	E_1E_2	
a_{12}	OA_1, OA_2	0.057 m
L_{1i}	O_iM_i, i = 1 to 6	$L_{11} = L_{12} = L_{14} = L_{15} = 0.155$m $L_{13} = L_{16} = 0.205$ m
L_{2i}	M_iP_i, i = 1 to 6	$L_{21} = L_{22} = L_{24} = L_{25} = 0.185$m $L_{23} = L_{26} = 0.185$ m

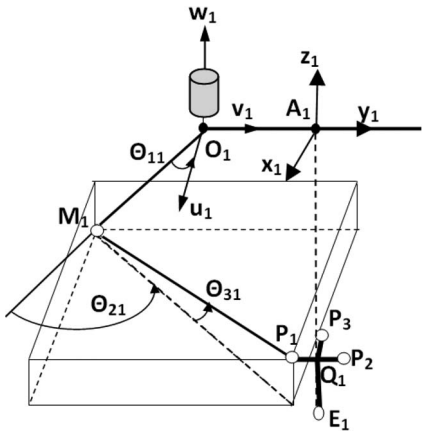

Fig. 6. Coordinate systems of the local leg coordinate.

to O_iM_i line. Joint angles, θ_{2i} and θ_{3i} are measured from the extended line of O_iM_i to the interaction of the vertical plane included M_iP_i and the $O_iu_iv_i$ plane, and from the interaction line to M_iP_i, respectively.

The local leg position vectors $\overrightarrow{O_iP_i}$ for six legs satisfy the vector equations

$$\overrightarrow{O_iP_i} = \overrightarrow{O_iM_i} + \overrightarrow{M_iP_i}. \tag{1}$$

Six leg equations for the position $\overrightarrow{O_iP_i}$ $(i = 1, \ldots, 6)$ are derived from (1)

$$\overrightarrow{O_iP_i} = \begin{bmatrix} P_{ui} \\ P_{vi} \\ P_{wi} \end{bmatrix} = \begin{bmatrix} L_{1i}\cos\theta_{1i} + L_{2i}\cos\theta_{3i}\cos(\theta_{1i}+\theta_{2i}) \\ L_{1i}\sin\theta_{1i} + L_{2i}\cos\theta_{3i}\sin(\theta_{1i}+\theta_{2i}) \\ L_{2i}\sin\theta_{3i} \end{bmatrix}. \tag{2}$$

The position vector of the upper end effector defined on $A_1x_1y_1z_1$ is $A_1E_1 = [x_1\ y_1\ z_1]^T$. The upper local leg position vectors $\overrightarrow{O_iP_i}$ $(i = 1, 2, 3)$ are converted to the upper leg position vectors O_iP_i defined on the upper base coordinate $A_1x_1y_1z_1$ by the coordinate transformation matrix T_i

$$O_iP_i = T_i\overrightarrow{O_iP_i} \tag{3}$$

where

$$T_1 = T_2 = \begin{bmatrix} 1 & 0 & 0 \\ 0 & 1 & 0 \\ 0 & 0 & 1 \end{bmatrix}, \quad T_3 = \begin{bmatrix} 1 & 0 & 0 \\ 0 & 0 & 1 \\ 0 & -1 & 0 \end{bmatrix}.$$

The position vectors, A_1P_i $(i = 1, 2, 3)$ then satisfy a vector equation defined on the upper base coordinate $A_1x_1y_1z_1$

$$A_1P_i = A_1O_i + O_iP_i = A_1E_1 + E_1Q_1 + Q_1P_i. \tag{4}$$

The position vector A_1P_i are then expressed as

$$\begin{bmatrix} 0 \\ -a \\ 0 \end{bmatrix} + \begin{bmatrix} 1 & 0 & 0 \\ 0 & 1 & 0 \\ 0 & 0 & 1 \end{bmatrix} \begin{bmatrix} P_{u1} \\ P_{v1} \\ P_{w1} \end{bmatrix} = \begin{bmatrix} x_1 \\ y_1 \\ z_1 \end{bmatrix} + \begin{bmatrix} 0 \\ 0 \\ h \end{bmatrix} + \begin{bmatrix} 0 \\ -d \\ 0 \end{bmatrix} \tag{5}$$

$$\begin{bmatrix} 0 \\ a \\ 0 \end{bmatrix} + \begin{bmatrix} 1 & 0 & 0 \\ 0 & 1 & 0 \\ 0 & 0 & 1 \end{bmatrix} \begin{bmatrix} P_{u2} \\ P_{v2} \\ P_{w2} \end{bmatrix} = \begin{bmatrix} x_1 \\ y_1 \\ z_1 \end{bmatrix} + \begin{bmatrix} 0 \\ 0 \\ h \end{bmatrix} + \begin{bmatrix} 0 \\ d \\ 0 \end{bmatrix} \tag{6}$$

$$\begin{bmatrix} -b \\ 0 \\ c \end{bmatrix} + \begin{bmatrix} 1 & 0 & 0 \\ 0 & 0 & 1 \\ 0 & -1 & 0 \end{bmatrix} \begin{bmatrix} P_{u3} \\ P_{v3} \\ P_{w3} \end{bmatrix} = \begin{bmatrix} x_1 \\ y_1 \\ z_1 \end{bmatrix} + \begin{bmatrix} 0 \\ 0 \\ h \end{bmatrix} + \begin{bmatrix} -d \\ 0 \\ 0 \end{bmatrix}. \tag{7}$$

Equations (5)–(7) are reformulated as

$$\begin{bmatrix} L_{21}\cos\theta_{31}\cos(\theta_{11}+\theta_{21}) \\ L_{21}\cos\theta_{31}\sin(\theta_{11}+\theta_{21}) \\ L_{21}\sin\theta_{31} \end{bmatrix} = \begin{bmatrix} x_1 - L_{11}\cos\theta_{11} \\ y_1 - d + a - L_{11}\sin\theta_{11} \\ z_1 + h \end{bmatrix} \tag{8}$$

$$\begin{bmatrix} L_{22}\cos\theta_{32}\cos(\theta_{12}+\theta_{22}) \\ L_{22}\cos\theta_{32}\sin(\theta_{12}+\theta_{22}) \\ L_{22}\sin\theta_{32} \end{bmatrix} = \begin{bmatrix} x_1 - L_{12}\cos\theta_{12} \\ y_1 + d - a - L_{12}\sin\theta_{12} \\ z_1 + h \end{bmatrix} \tag{9}$$

$$\begin{bmatrix} L_{23}\cos\theta_{33}\cos(\theta_{13}+\theta_{23}) \\ L_{23}\sin\theta_{33} \\ L_{23}\cos\theta_{33}\sin(\theta_{13}+\theta_{23}) \end{bmatrix} = \begin{bmatrix} x_1 - d + b - L_{13}\sin\theta_{13} \\ y_1 \\ -z_1 + c - h - L_{13}\sin\theta_{13} \end{bmatrix}. \tag{10}$$

Three leg equations for the upper structure are firstly derived and solved to find the position of the upper end effector.

The sphere equations of three legs are obtained by summing squares of scalar equations in (8)–(10) as

$$\begin{aligned} L_{21}^2 &= x_1^2 + y_1^2 + z_1^2 + 2[A_1x_1 + B_1y_1 + C_1z_1] \\ &\quad + A_1^2 + B_1^2 + C_1^2 \\ L_{22}^2 &= x_1^2 + y_1^2 + z_1^2 + 2[A_2x_1 + B_2y_1 + C_2z_1] \\ &\quad + A_2^2 + B_2^2 + C_2^2 \\ L_{23}^2 &= x_1^2 + y_1^2 + z_1^2 + 2[A_3x_1 + B_3y_1 + C_3z_1] \\ &\quad + A_3^2 + B_3^2 + C_3^2 \end{aligned} \tag{11}$$

where

$$\begin{aligned} &A_1 = -L_{11}\cos\theta_{11}, \quad A_2 = -L_{12}\cos\theta_{12}, \\ &A_3 = -d + b - L_{13}\cos\theta_{13} \\ &B_1 = -d + a - L_{11}\sin\theta_{11}, \\ &B_2 = d - a - L_{12}\sin\theta_{12}, \quad B_3 = 0 \\ &C_1 = h, \quad C_2 = h, \quad C_3 = -c + h + L_{13}\sin\theta_{13}. \end{aligned}$$

The first plane equation is obtained by subtracting the first and second sphere equations of (11). Similarly the second plane equation is determined by subtracting the second and third sphere equations of (11)

$$\begin{aligned} A_{12}x_1 + B_{12}y_1 + C_{12}z_1 + D_{12} &= 0 \\ A_{23}x_1 + B_{23}y_1 + C_{23}z_1 + D_{23} &= 0 \end{aligned} \tag{12}$$

where

$$\begin{aligned} &A_{12} = 2(A_1 - A_2),\ B_{12} = 2(B_1 - B_2),\ C_{12} = 2(C_1 - C_2) \\ &D_{12} = A_1^2 - A_2^2 + B_1^2 - B_2^2 + C_1^2 - C_2^2 - L_{21}^2 + L_{22}^2 \\ &A_{23} = 2(A_2 - A_3),\ B_{23} = 2(B_2 - B_3),\ C_{23} = 2(C_2 - C_3) \\ &D_{23} = A_2^2 - A_3^2 + B_2^2 - B_3^2 + C_2^2 - C_3^2 - L_{22}^2 + L_{23}^2. \end{aligned}$$

The two plane equations of (12) determine an interaction line as

$$\begin{cases} z_1 = a_1x_1 + b_1 \\ y_1 = a_2x_1 + b_2 \end{cases} \tag{13}$$

where

$$\begin{aligned} a_1 &= \frac{B_{12}A_{23} - B_{23}A_{12}}{B_{23}C_{12} - B_{12}C_{23}}, \quad b_1 = \frac{B_{12}D_{23} - B_{23}D_{12}}{B_{23}C_{12} - B_{12}C_{23}} \\ a_2 &= \frac{A_{23}C_{12} - A_{12}C_{23}}{B_{12}C_{23} - B_{23}C_{12}}, \quad b_2 = \frac{D_{23}C_{12} - D_{12}C_{23}}{B_{12}C_{23} - B_{23}C_{12}}. \end{aligned}$$

Inserting an interaction line of (13) into the first sphere equation of (11) leads to

$$\begin{aligned} L_{21}^2 &= x_1^2 + y_1^2 + z_1^2 + 2[A_1x_1 + B_1y_1 + C_1z_1] \\ &\quad + A_1^2 + B_1^2 + C_1^2 \\ &= x_1^2 + (a_2x_1 + b_2)^2 + (a_2x_1 + b_1)^2 \\ &\quad + 2\left[A_1x_1 + B_1(a_2x_1 + b_2) + C_1(a_1x_1 + b_1)\right] \\ &\quad + A_1^2 + B_1^2 + C_1^2. \end{aligned} \tag{14}$$

Equation (14) is reformulated as

$$K_0x_1^2 + K_1x_1 + K_2 = 0 \tag{15}$$

where

$$\begin{aligned} &K_0 = 1 + a_1^2 + a_2^2 \\ &K_1 = 2a_1b_1 + 2a_2b_2 + 2A_1 + 2B_1a_2 + 2C_1a_1 \\ &K_2 = A_1^2 + B_1^2 + C_1^2 + b_1^2 + b_2^2 + 2B_1b_2 + 2C_1b_1 - L_{21}^2. \end{aligned}$$

In general, if $K_1^2 - 4K_0K_2 > 0$ then there are eight positions for the end effector of upper structure

$$\begin{aligned} x_1 &= \frac{-K_1 \pm \sqrt{K_1^2 - 4K_0K_2}}{2K_0} \\ y_1 &= a_2x_1 + b_2 \\ z_1 &= a_1x_1 + b_1. \end{aligned} \tag{16}$$

The position vector of the lower end effector defined on the lower coordinate system $A_2x_2y_2z_2$, $A_2E_2 = [x_2\ y_2\ z_2]^T$, can also be calculated in the same manner. The positions of upper and lower end effectors, E_1 and E_2, are transformed to the global base coordinate system OXYZ as

$$\begin{bmatrix} X_1 \\ Y_1 \\ Z_1 \end{bmatrix} = \begin{bmatrix} 1 & 0 & 0 \\ 0 & 1 & 0 \\ 0 & 0 & 1 \end{bmatrix} \begin{bmatrix} x_1 \\ y_1 \\ z_1 \end{bmatrix} + \begin{bmatrix} 0 \\ 0 \\ A_1A_2/2 \end{bmatrix} \tag{17}$$

$$\begin{bmatrix} X_2 \\ Y_2 \\ Z_2 \end{bmatrix} = \begin{bmatrix} 1 & 0 & 0 \\ 0 & -1 & 0 \\ 0 & 0 & -1 \end{bmatrix} \begin{bmatrix} x_2 \\ y_2 \\ z_2 \end{bmatrix} + \begin{bmatrix} 0 \\ 0 \\ -A_1A_2/2 \end{bmatrix}. \tag{18}$$

The main end effector of the 6-DOF haptic device is located at the center of the steering handle (E). The position of the center of the steering handle is then calculated as

$$x = \frac{X_1 + X_2}{2}, \quad y = \frac{Y_1 + Y_2}{2}, \quad z = \frac{Z_1 + Z_2}{2}. \tag{19}$$

Orientation angles of the steering handle,α, β, γ, are determined as

$$\alpha = \tan^{-1}\left(\frac{Y_1 - Y_2}{Z_1 - Z_2}\right),\ \beta = \tan^{-1}\left(\frac{X_1 - X_2}{Z_1 - Z_2}\right),\ \gamma = C(l - l_0) \tag{20}$$

where $l = \sqrt{(X_1 - X_2)^2 + (Y_1 - Y_2)^2 + (Z_1 - Z_2)^2}$ is the length of the steering handle, $l_{\max} = 0.20$ m, $l_0 = 0.14$ m$C = 2\pi/(l_{\max} - l_0)$.

B. Inverse Kinematics

Six active joint angles of the haptic device can be determined if the position and orientation of the main end effector are given. First, the position of the upper and lower end effectors can be calculated from the position and orientation of the main end effector as

$$\begin{aligned} X_1 &= x + l\tan(\beta)/\xi, \quad X_2 = x - l\tan(\beta)/\xi \\ Y_1 &= y + l\tan(\alpha)/\xi, \quad Y_2 = y - l\tan(\alpha)/\xi \\ Z_1 &= z + l/\xi, \quad Z_2 = z - l/\xi \end{aligned} \tag{21}$$

where

$$\begin{aligned} l &= \gamma/C + l_0 \\ \xi &= 2\sqrt{\tan^2(\alpha) + \tan^2(\beta) + 1}. \end{aligned}$$

Three active joint angles of the upper structure $\theta_u = [\theta_{11}\ \theta_{12}\ \theta_{13}]^T$ and three active joint angles of the lower structure $\theta_l = [\theta_{14}\ \theta_{15}\ \theta_{16}]^T$ can be separately calculated in the same

manner. Only inverse kinematics of the upper structure is then analyzed to find three active joint angles of the upper structure. Rotation angles, θ_{3i} can be easily calculated by (2) as

$$\theta_{3i} = \sin^{-1}\left(\frac{P_{wi}}{L_{2i}}\right). \tag{22}$$

Rotation angles θ_{2i} can be obtained by summing the squares of the three components in (2)

$$\theta_{2i} = \cos^{-1}\left(\frac{P_{ui}^2 + P_{vi}^2 + P_{wi}^2 - L_{1i}^2 - L_{2i}^2}{2L_{1i}L_{2i}\cos\theta_{3i}}\right). \tag{23}$$

The joint angles θ_{1i} can be determined from the first and second components in (2)

$$\theta_{1i} = \tan^{-1}\left(\frac{-L_{2i}c\theta_{3i}s\theta_{2i}P_{ui} + (L_{1i} + L_{2i}c\theta_{3i}c\theta_{2i})P_{vi}}{(L_{1i} + L_{2i}c\theta_{3i}c\theta_{2i})P_{ui} + L_{2i}c\theta_{3i}s\theta_{2i}P_{vi}}\right) \tag{24}$$

where $c\theta_i = \cos\theta_i$, $s\theta_i = \sin\theta_i$.

IV. Static Force Analysis

Jacobian matrix of the 6-DOF haptic device is determined from a combination of two Jacobian matrices of the upper and lower structures. First, Jacobian of the upper structure is analyzed. The closed position vector equations for each leg of the upper structure ($i = 1, 2, 3$) are described on the global base coordinate system OXYZ as

$$\overrightarrow{OE_1} = \overrightarrow{OA_1} + \overrightarrow{A_iO_i} + \overrightarrow{O_iM_i} + \overrightarrow{M_iP_i} + \overrightarrow{P_iQ_1} + \overrightarrow{Q_1E_1}. \tag{25}$$

Differentiating (25) with respect to time leads to

$$\frac{d\overrightarrow{OE_1}}{dt} = \frac{d\overrightarrow{O_iM_i}}{dt} + \frac{d\overrightarrow{M_iP_i}}{dt} \tag{26}$$

where

$$\frac{d}{dt}(\overrightarrow{OA_1} + \overrightarrow{A_1O_i} + \overrightarrow{P_iQ_1} + \overrightarrow{Q_1E_1}) = 0.$$

Equation (26) can be rewritten by using rigid body dynamics as

$$V_{E1} = \omega_{1i} \times \overrightarrow{O_iM_i} + \omega_{2i} \times \overrightarrow{M_iP_i} \tag{27}$$

where $V_{E1} = [V_{1x}\ V_{1y}\ V_{1z}]^T$ is the translational velocity of E_1 on the global base coordinate system. ω_{1i} is the angular velocity of the first link of each leg. ω_{2i} is the angular velocity of the second link of each leg. Applying dot product of $\overrightarrow{M_iP_i}$ on (27) to eliminate ω_{2i} leads to

$$V_{E1} \cdot \overrightarrow{M_iP_i} = \omega_{1i} \cdot (\overrightarrow{O_iM_i} \times \overrightarrow{M_iP_i}) \tag{28}$$

where

$$\omega_{1i} = [0\ 0\ \dot{\theta}_{1i}]^T, \quad \overrightarrow{O_iM_i} = L_{1i}[c\theta_{1i}\ s\theta_{1i}\ 0]^T$$
$$\overrightarrow{M_iP_i} = L_{2i}[c\theta_{3i}\ c\theta_{1i+2i}\ c\theta_{3i}s\theta_{1i+2i}\ s\theta_{3i}]^T \tag{29}$$

and where

$$c\theta_i = \cos\theta_i, \quad s\theta_i = \sin\theta_i$$
$$c\theta_{i+j} = c(\theta_i + \theta_j), \quad s\theta_{i+j} = s(\theta_i + \theta_j).$$

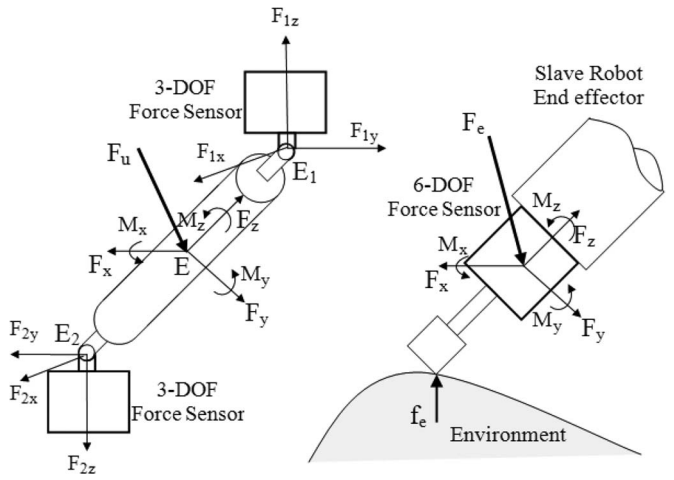

Fig. 7. Force coordinate systems on the handle and the slave robot.

The relation between the translational velocity of E_1, V_{E1}, and the joint angular velocity of the upper structure, $\dot{\theta}_u = [\dot{\theta}_{11}\ \dot{\theta}_{12}\ \dot{\theta}_{13}]^T$, can be obtained by substituting (29) into (28) and reformulating (28)

$$V_{E1} = J_1^{-1}\dot{\theta}_u \tag{30}$$

where Jacobian matrix of upper structure J_1 is defined as

$$J_1 = J_{\theta 1}^{-1}J_{x1}$$
$$J_{x1} = \begin{bmatrix} c\theta_{31}c\theta_{11+21} & c\theta_{31}s\theta_{11+21} & s\theta_{31} \\ c\theta_{32}c\theta_{12+22} & c\theta_{32}s\theta_{12+22} & s\theta_{32} \\ c\theta_{33}c\theta_{13+23} & s\theta_{33} & -c\theta_{33}s\theta_{13+23} \end{bmatrix}$$
$$J_{\theta 1} = \begin{bmatrix} L_{11}c\theta_{31}s\theta_{21} & 0 & 0 \\ 0 & L_{12}c\theta_{32}s\theta_{22} & 0 \\ 0 & 0 & L_{13}c\theta_{33}s\theta_{23} \end{bmatrix}. \tag{31}$$

Similarly $V_{E2} = [V_{2x}\ V_{2y}\ V_{2z}]^T$ is the translational velocity of E_2 on the global base coordinate system. The relation between the translational velocity of E_2 and the joint angular velocity of the lower structure $\dot{\theta}_l = [\dot{\theta}_{14}\ \dot{\theta}_{15}\ \dot{\theta}_{16}]^T$ is expressed as

$$V_{E2} = J_2^{-1}\dot{\theta}_l \tag{32}$$

where Jacobian matrix of the lower structure J_2 is defined as

$$J_2 = J_{\theta 2}^{-1}J_{x2}$$
$$J_{x2} = \begin{bmatrix} c\theta_{34}c\theta_{14+24} & c\theta_{34}s\theta_{14+24} & s\theta_{34} \\ c\theta_{35}c\theta_{15+25} & c\theta_{35}s\theta_{15+25} & s\theta_{35} \\ c\theta_{36}c\theta_{16+26} & s\theta_{36} & -c\theta_{36}s\theta_{16+26} \end{bmatrix}$$
$$J_{\theta 2} = \begin{bmatrix} L_{14}c\theta_{34}s\theta_{24} & 0 & 0 \\ 0 & L_{15}c\theta_{35}s\theta_{25} & 0 \\ 0 & 0 & L_{16}c\theta_{36}s\theta_{26} \end{bmatrix}. \tag{33}$$

Force coordinate systems of the steering handle and the slave robot are shown in Fig. 7. Two 3-DOF force sensors are installed on the end effectors of upper and lower structures at $E_1F_{1x}F_{1y}F_{1z}$ and $E_2F_{2x}F_{2y}F_{2z}$. A 6-DOF force sensor is attached on the end effector of the serial robot. The torque/force of the handle F_u applied by users can be measured with two 3-DOF force sensors.

The relationship between the torque/force vector of the handle and force vectors at the upper and lower end effectors is described as

$$F_u = LF_{12} \tag{34}$$

where

$$L = L_1 L_2,$$

$$L_1 = \begin{bmatrix} 0 & -l/2 & 0 & 0 & -l/2 & 0 \\ l/2 & 0 & 0 & -l/2 & 0 & 0 \\ 0 & 0 & k & 0 & 0 & k \\ 1 & 0 & 0 & 1 & 0 & 0 \\ 0 & 1 & 0 & 0 & -1 & 0 \\ 0 & 0 & 1 & 0 & 0 & -1 \end{bmatrix},$$

$$L_2 = \begin{bmatrix} c\beta & s\alpha s\beta & -c\alpha s\beta & 0 & 0 & 0 \\ 0 & c\alpha & s\alpha & 0 & 0 & 0 \\ s\beta & -s\alpha c\beta & c\alpha c\beta & 0 & 0 & 0 \\ 0 & 0 & 0 & c\beta & s\alpha s\beta & -c\alpha s\beta \\ 0 & 0 & 0 & 0 & c\alpha & s\alpha \\ 0 & 0 & 0 & s\beta & -s\alpha c\beta & c\alpha c\beta \end{bmatrix}.$$

$F_u = [M_x \ M_y \ M_z \ F_x \ F_y \ F_z]^T$ is the torque/force vector described in the handle fixed coordinate and $F_{12} = [F_{1x} \ F_{1y} \ F_{1z} \ F_{2x} \ F_{2y} \ F_{2z}]^T$ is the force vector in the upper and lower end effectors. The upper and lower end effectors are kinematically constrained to move only translational directions. k is a gain represented the relationship between moment M_z with respect to forces F_{1z} and F_{2z}. The value of k is obtained by experiments. L_1 denotes the relationship between the 3-DOF forces at two end effectors and the 6-DOF torque/force of the handle when orientation angles of α, β are equal to zero. L_2 denotes the Euler angles between the handle fixed coordinate system and the global coordinate system. Active joint torque vector is defined as

$$\tau_c = \begin{bmatrix} \tau_t \\ \tau_b \end{bmatrix} \tag{35}$$

where $\tau_t = [\tau_1 \ \tau_2 \ \tau_3]^T$ and $\tau_b = [\tau_4 \ \tau_5 \ \tau_6]^T$.

The force vector at the upper and lower end effectors is described as

$$F_{12} = \hat{J}_h \tau_c \tag{36}$$

where

$$\hat{J}_h = \begin{bmatrix} J_1^T & 0 \\ 0 & J_2^T \end{bmatrix}.$$

Combining (34) and (36) leads to the relationship between the torque/force vector at the handle fixed coordinate and the joint torque vector

$$F_u = J_h^T \tau_c \tag{37}$$

where the Jacobian is

$$J_h = \hat{J}_h^T L^T \tag{38}$$

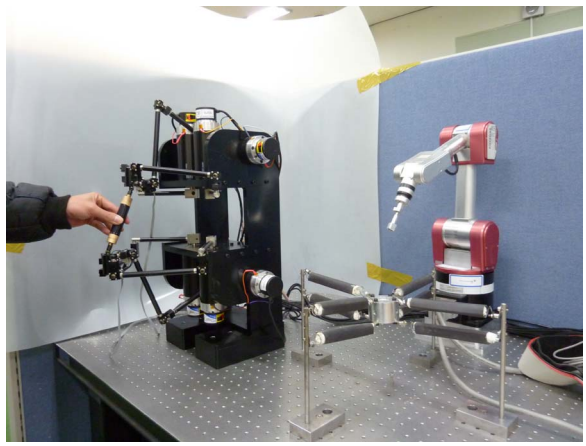

Fig. 8. Test rig of teleoperation system.

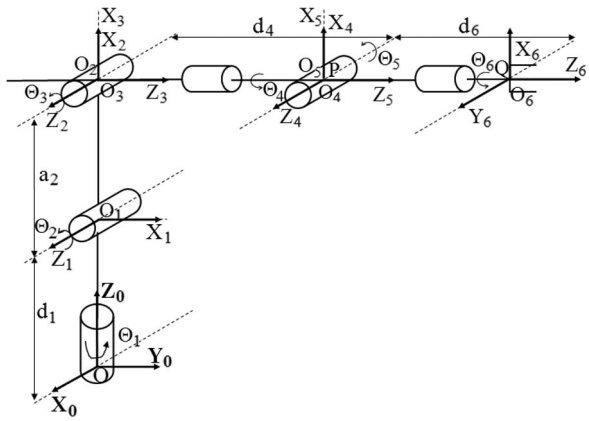

Fig. 9. Schematic of the 6 DOF serial robot.

TABLE II
DH PARAMETER OF 6-DOF SERIAL ROBOT

Link	a_i	α_i	d_i	Θ_i	Initial value
1	0	90°	d_1 = 0.26 m	Θ_1	90°
2	a_2 = 0.25 m	0	0	Θ_2	90°
3	0	90°	0	Θ_3	0
4	0	-90°	d_4 = 0.24 m	Θ_4	0
5	0	90°	0	Θ_5	0
6	0	0	d_6 = 0.14 m	Θ_6	0

The force coordinate of the contact force F_e fixed at the slave robot has the same orientation as the handle coordinate since the end effector of the slave robot should tract the steering handle. The contact force F_e is measured from the 6-DOF force sensor when the end effector of the slave robot contacts environment.

V. TELEOPERATION CONTROL SYSTEM

The teleoperation test rig shown in Fig. 8 consists of a master device (a new 6-DOF haptic device), a slave robot (a 6-DOF serial robot) and the tele-operation controller. Users can manipulate the steering handle and apply forces/torques (F/T) to generate movements. The serial robot used in this teleoperation system has six revolute joints shown in Fig. 9 and its DH parameters are shown in Table II.

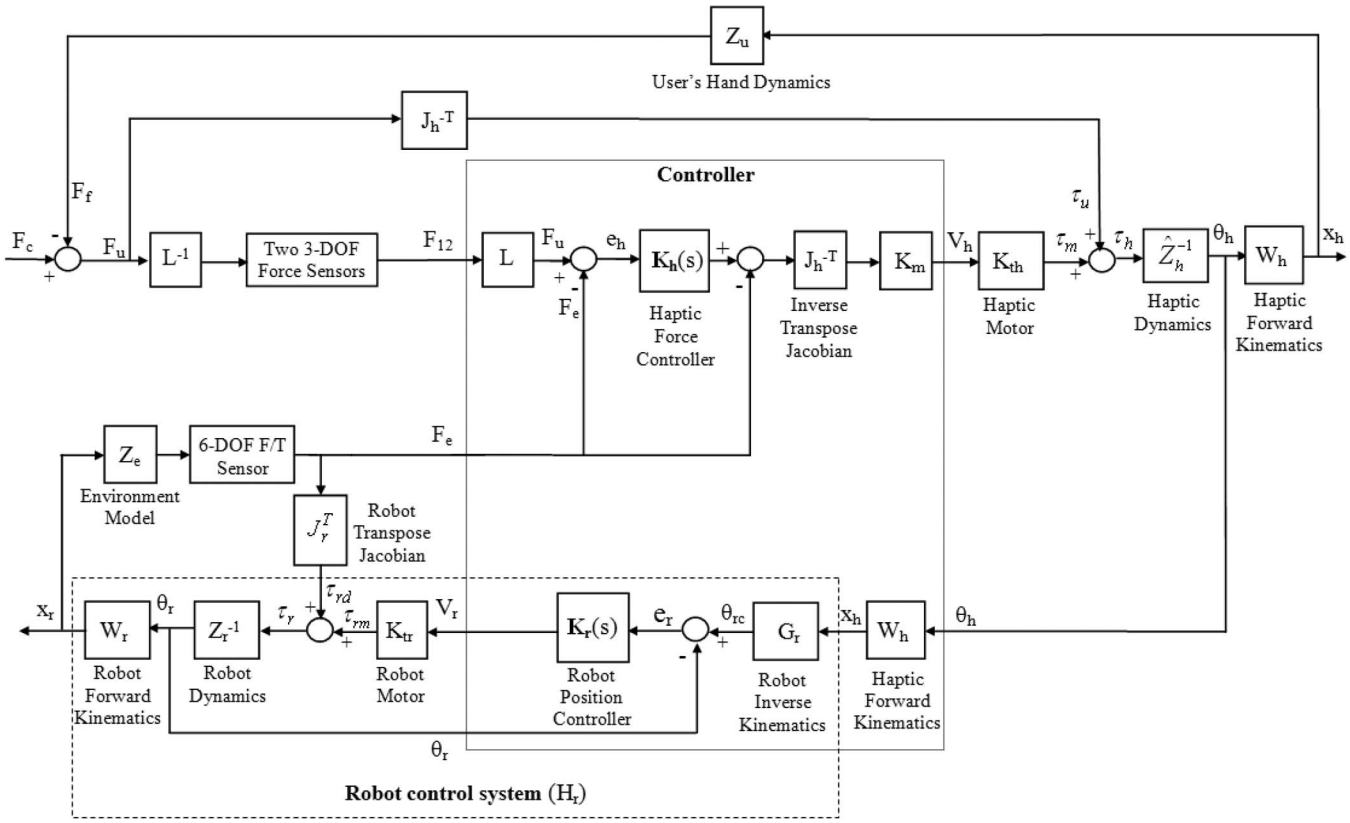

Fig. 10. Implemented teleoperation control system.

The teleoperation control system is shown in Fig. 10. The teleoperation control system can be divided into two main parts: position control of slave serial robot and force control of master haptic device. Users can hold the handle of haptic device and generate motions. The motions of the handle are measured by encoders. These joint angles are used to calculate forward kinematics of haptic device so that its trajectory is determined. This trajectory is composed of three positions and three rotations of the center of the handle. The slave serial robot uses this trajectory to find joint angle commands, $\theta_{\rm rc}$ through inverse kinematics $G_{\rm r}$. The error between the command, $\theta_{\rm rc}$ and feedback, $\theta_{\rm r}$ joint angles is the input of position controller, $K_{\rm r}(s)$. Its output is converted into voltage commands, $V_{\rm r}$ for the robot's motors. The rotations of robot joints determine the trajectory of end effector, $x_{\rm r}$. There exist some tracking errors because of robot dynamics. When the slave serial robot is manipulated, its end effector may touch the environment $Z_{\rm e}$. The contacting force, $F_{\rm e}$, is mechanically transmitted to the joints of robot through its transpose Jacobian matrix J_r^T. This force works as the external disturbances so it may reduce tracking performances of the robot.

The user force F_u is the sum of the feedback force by the user hand F_f and the command force F_c to generate movements of the haptic device. When the user force is applied on the center of the handle, it is converted to the forces F_{12} at the upper and lower end effectors by the transformation matrix L^{-1}. The forces F_{12} are measured by two 3-DOF force sensors. The user force F_u is also mechanically transmitted to the joint torque τ_u by the Jacobian matrix of J_h.

The user manipulating the haptic device should feel actual contact force from the environment not those of the structure of the haptic device. Detecting the actual contact force from environment by using a haptic device may present a hardware design problem such as low inertia and frictions.

The closed loop force control can also be used to reduce undesired dynamic effects from the haptic device. Teleoperation system with the open loop force control and the closed loop force control is shown in Fig. 11. For the open loop force control the contact force F_e from environment is directly converted to the motor forces τ_m. The user then may feel the contact forces as well as undesired haptic dynamic forces due to inertia, joint frictions, and gravity.

The closed loop force control implies that the force controller $K_h(s)$ is added to the control system. The inputs of the controller are the force command F_e from the environment and the measured force F_u on the haptic device. Additional force sensors to measure the user force are then required for the closed loop force control. The closed loop force control system is analyzed to evaluate the performance of the controller. The total torque τ_h to the motor joints of the haptic device is described as

$$\tau_h = \tau_m + \tau_u \tag{39}$$

where τ_m and τ_u are motor torque and user applied torque, respectively. The gain K_m shown in Fig. 10 is a scale factor to convert required motor torques into voltage commands such

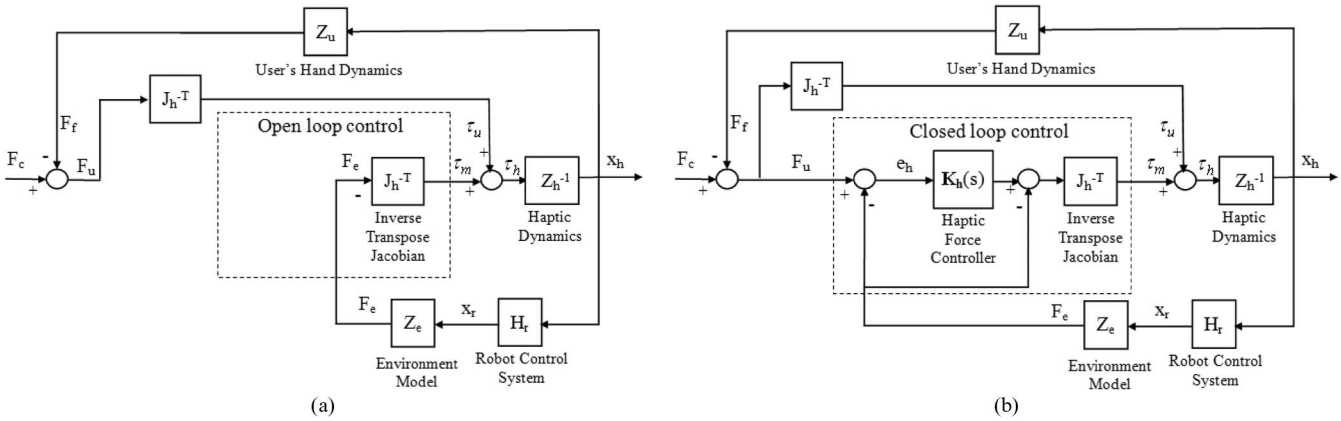

Fig. 11. Impedance force control for teleoperation. (a) Open loop force control; (b) closed loop force control.

that $K_m K_{th}$ is equal to 1. The motor torque τ_m and the user torque τ_u are calculated as

$$\tau_m = J_h^{-T}\left[K_h F_u - (I + K_h)F_e\right]$$
$$\tau_u = J_h^{-T} F_u \tag{40}$$

where I is the identity matrix. Impedance model of the haptic device is described as

$$\tau_h = \hat{Z}_h W_h^{-1} X_h = Z_h X_h. \tag{41}$$

Combining (39)–(41) leads to the force error equation

$$e_h = F_u - F_e = (I + K_h)^{-1} J_h^T Z_h X_h. \tag{42}$$

Equation (42) implies that the dynamic effects of the haptic device can be reduced by increasing the controller gain of $K_h(s)$.

If controller gains are adjusted as high as possible, the user should be able to feel free of dynamics during the free motion with no external force and the user should be able to feel the exact contacting forces during the contacts. However, the system becomes unstable if high control gains are selected [23]. For open loop control with $K_h(s) = 0$, the force error leads to exactly the same as the haptic dynamics

$$e_h = J_h^T Z_h X_h. \tag{43}$$

Impedance models of the environment and user hand are expressed as

$$F_e = Z_e H_r X_h$$
$$F_f = Z_u X_h$$
$$F_u = F_c - F_f. \tag{44}$$

The closed loop impedance at the haptic device is calculated when (44) are inserted into (42)

$$\frac{X_h}{F_c} = \frac{1}{Z_e H_r + Z_u + (I + K_h)^{-1} J_h^T Z_h}. \tag{45}$$

The closed loop impedance implies that the dynamics of the haptic device can be reduced by adjusting the control gain of $K_h(s)$. The force control law for the teleoperation system is selected as a simple PID control

$$k_h(s) = k_p + k_d s + k_i/s. \tag{46}$$

The force controller for the 6-DOF haptic device is then described as

$$K_h(s) = diag\left([k_h, k_h, k_h, k_h, k_h, k_h]\right). \tag{47}$$

VI. Experiments

The closed loop force control algorithm using a conventional PID controller was developed and implemented on the digital controller. The closed loop control for free motions of the haptic device was first tested to evaluate the reduction of disturbance forces such as frictions, inertia and gravity. No contact force from the environment $(F_e = 0)$ is applied during the free motion. The proportional-derivative-integral control gains of k_p, k_d, k_i were selected to be 1.2, 0.0011, and 0.36, respectively.

The open loop control for free motions of the haptic device was also tested. The open loop control of the haptic device for free motions means that the haptic device is mechanically manipulated without any motor control. The measured user force F_u for open loop control of free motions is considered to be purely the dynamic forces caused by the haptic device. Shaking motions of the steering handle were generated for the closed loop force control of free motions. Very much the same shaking motions of the steering handle were also generated for the open loop force control of free motions. The trajectories of the steering handle for both the closed loop control and the open loop control are shown in Fig. 12. The user applied forces F_u for both the open loop control and the closed loop control were measured and compared as shown in Fig. 13.

Fig. 13 shows that the amplitude of the user force for the closed loop control is reduced by more than 60% compared to that for the open loop control. This implies that the dynamic forces caused by the haptic device can be reduced by the control

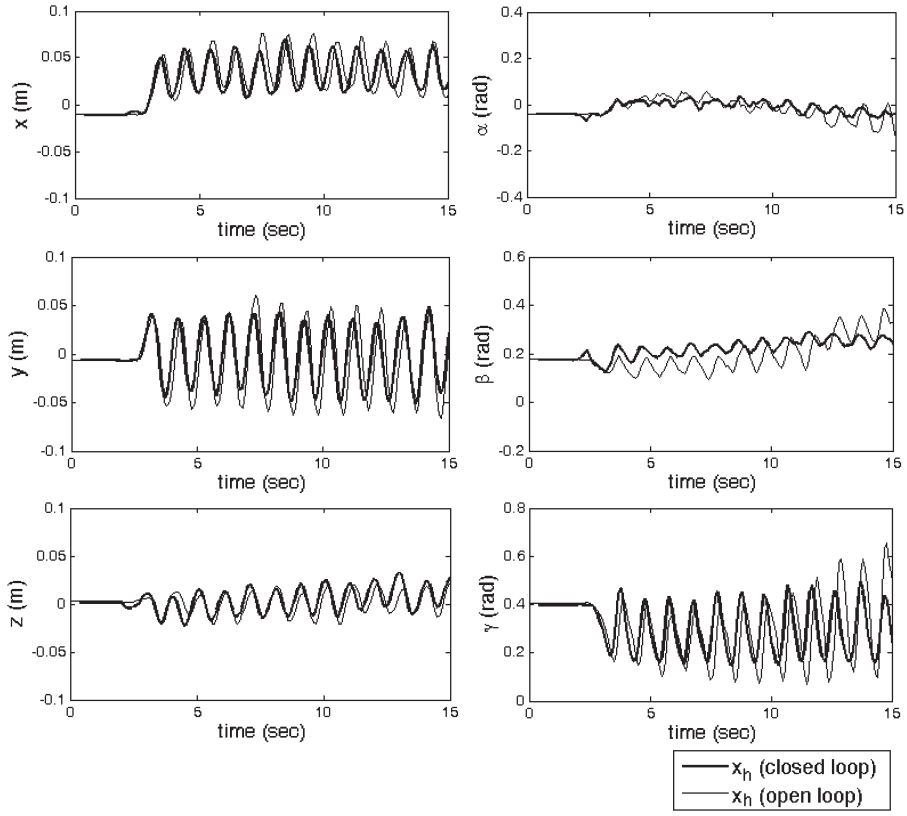

Fig. 12. Trajectory comparisons of haptic device in free motions.

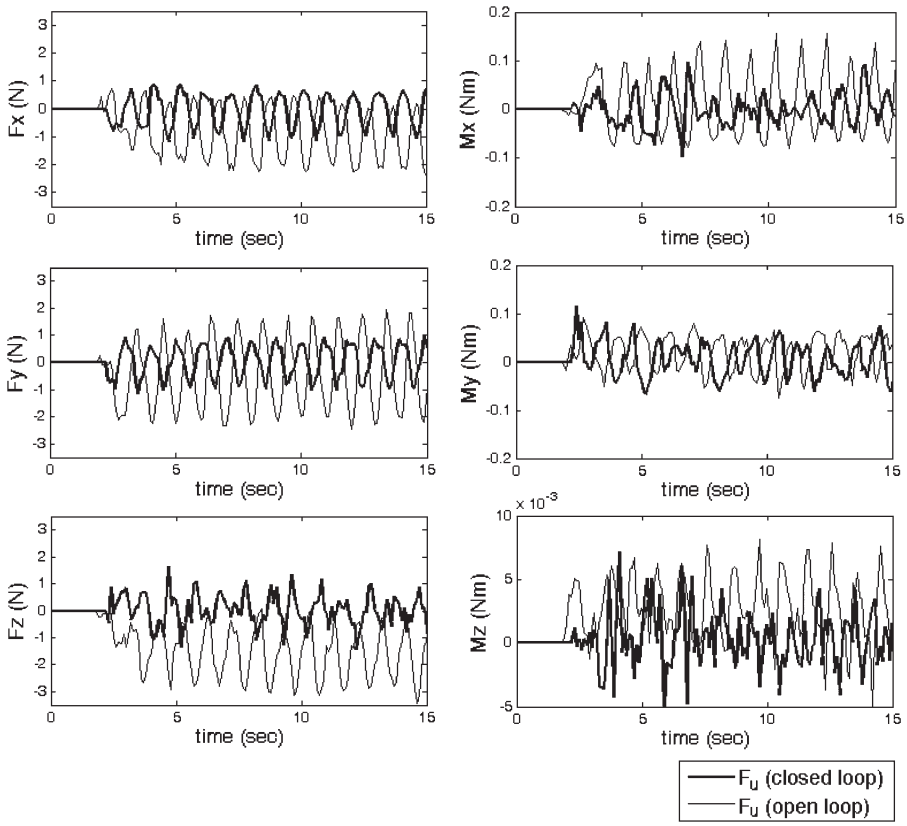

Fig. 13. User applied force comparisons of haptic device in free motions.

actions of the haptic motors. It is also interesting to see that the static force components of gravity for the open loop control in Fig. 13 are eliminated when the closed loop control is applied. This means that the integral controller may compensate static forces of gravity. However, increasing control gains of k_p, k_d, k_i resulted in more vibrations.

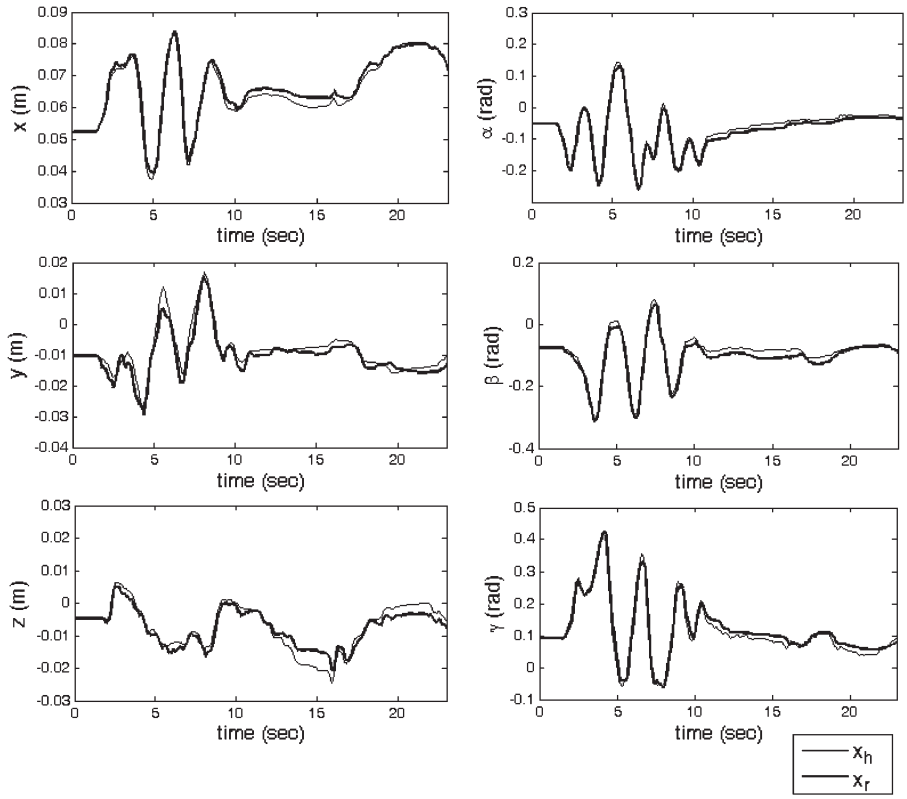

Fig. 14. Trajectory responses in open loop force control for teleoperation.

The force control system for teleoperation including the interaction with the environment was also tested. The position control of the 6-DOF serial robot using the new haptic device was performed to obtain the trajectory data of the robot manipulator. During the teleoperation the serial robot contact the environment. The contact force F_e from the environment could be compared with the user applied force F_u.

The open loop force control for teleoperation including the interaction with the environment was tested when the force controller of K_h in Fig. 10 was set to zero. The trajectory x_r of the slave robot was compared with the trajectory x_h of the haptic device for the open loop force control as shown in Fig. 14. The trajectory of the serial robot was well matched with that of the haptic device. There exist some trajectory errors between the slave robot and the haptic device since the contact force from the environment was applied at about 12 seconds after recording data. The contact force works as static force disturbances to the slave robot. Measured forces for the open loop force control are shown in Fig. 15.

The user applied forces F_u of the haptic device sensed from the 3 axis force sensors were compared with contact forces F_e sensed by the 6 axis F/T sensor. In Fig. 15 there exists substantial amount of force errors between the user applied forces and the contact forces largely due to the friction, gravity and inertia. These force errors implies that dynamic forces from the haptic device as well as the contact forces were felt by the user.

The closed loop force control for teleoperation including the interaction with the environment was tested when PID controller of K_h was applied. The trajectory x_r of the slave robot manipulator and the trajectory x_h of the haptic device for the closed loop force control are shown in Fig. 16.

The user applied forces F_u of the steering handle could track the contact forces F_e from environment well as shown in Fig. 17. This implies that the dynamic forces caused by manipulating the haptic device were also well compensated by the control actions of the haptic motors.

However, the closed loop force control produced some noise in forces because of the control actions and noise from the force sensors.

VII. Conclusion

A new 6-DOF haptic device is designed and analyzed. This haptic device has some unique features over previous designs. The designed 6-DOF parallel haptic device utilizes two 3-DOF parallel structures connected to each end of the steering handle by universal joints to provide 5-DOF motions (X, Y, Z, α, β). The steering handle provides one more DOF of twist motion (γ), since it is assembled with lead screws so that the rotation of the handle can be converted to linear motion. This parallel haptic device provides light moving frame and high stiffness so that quick motion may be obtained with large static forces. Since all six motors are fixed on the base frame, torque capacity of all motors can be freely selected while weights and inertias of the moving frame may be minimized. The new haptic device has unique six legged structure such that it provides large orientation angles. The orientation angle α about X-axis and

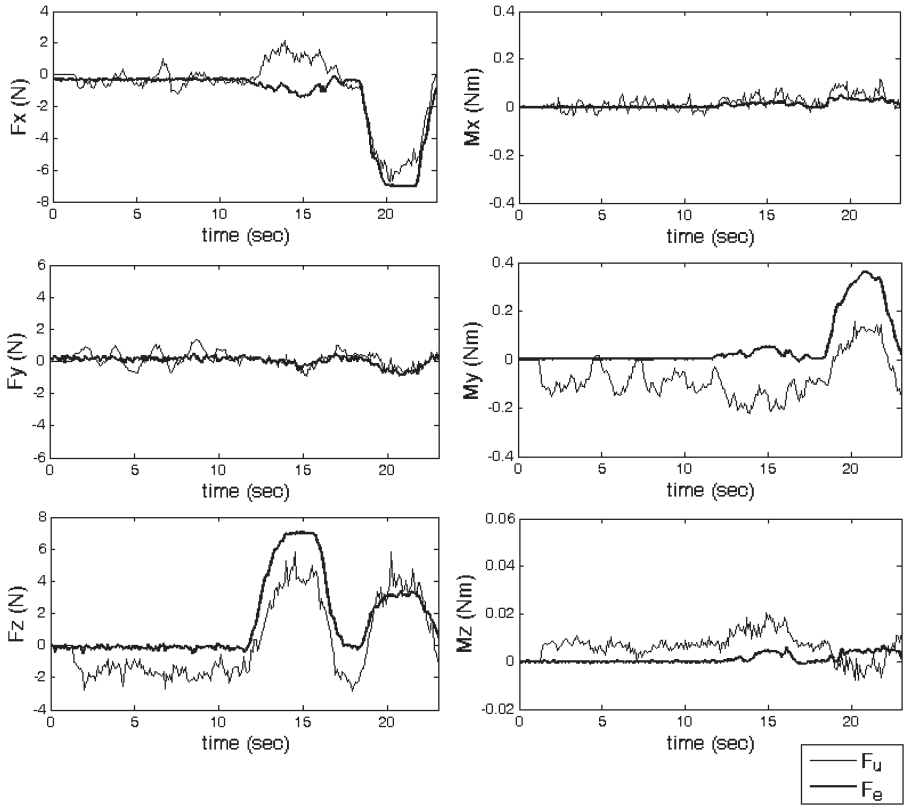

Fig. 15. Force responses in open loop force control for teleoperation.

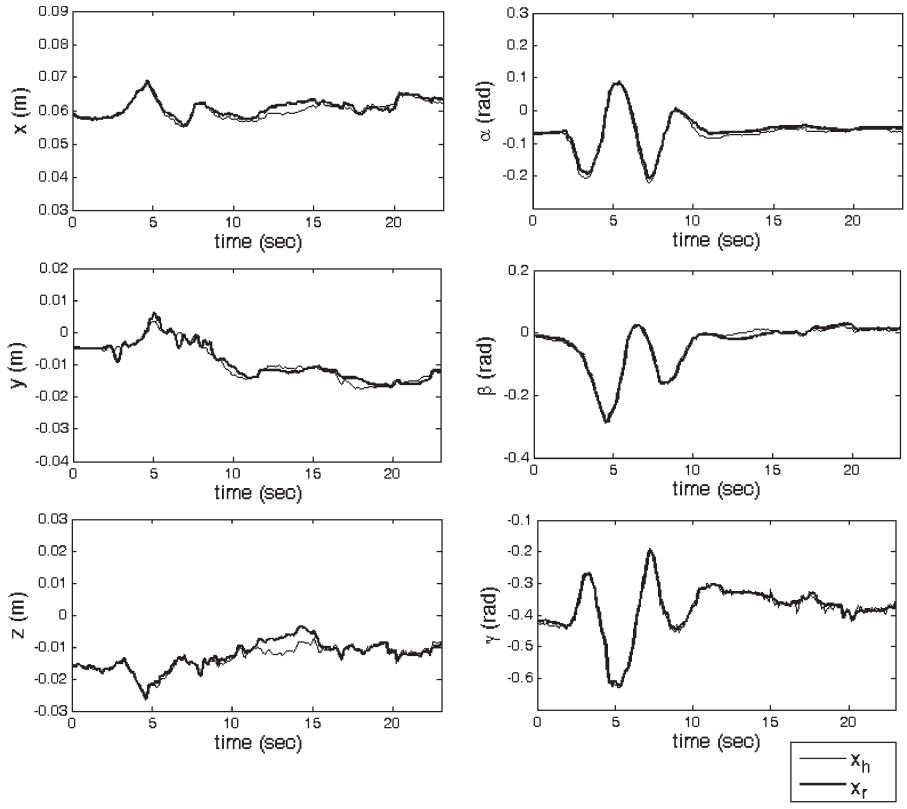

Fig. 16. Trajectory responses in closed loop force control for teleoperation.

angle β about Y-axis in the handle fixed coordinate are up to $\pm 90^\circ$. The twisting orientation angle (γ) by the steering handle is up to $\pm 180^\circ$. The orientation and position of the center of the handle are completely decoupled so that maximum orientation angles may be realized while the position is kept.

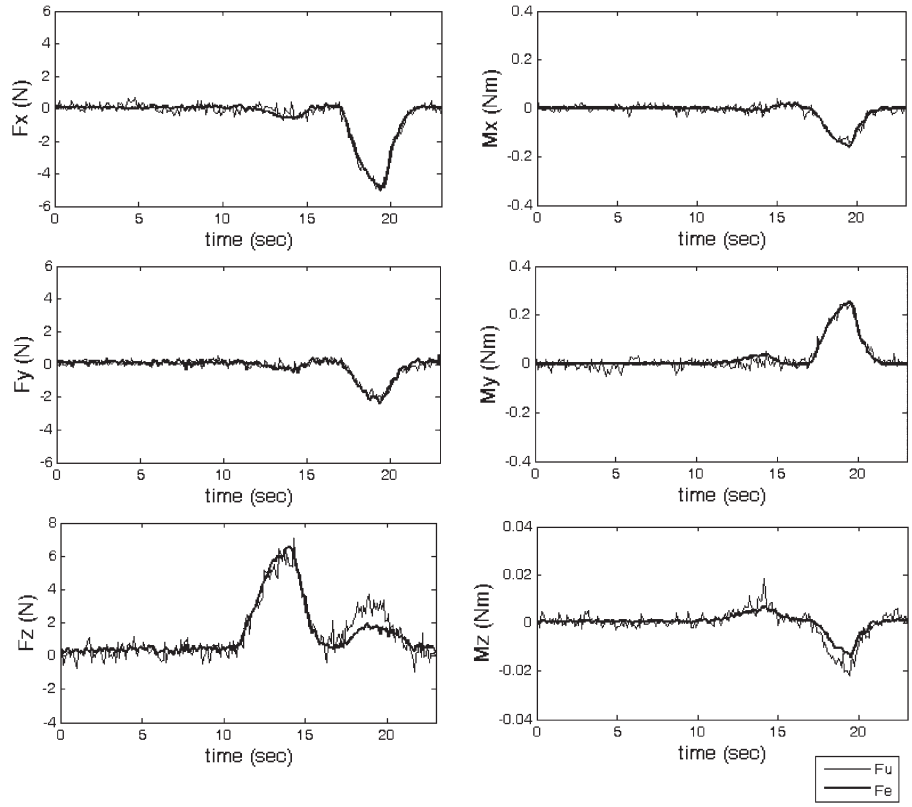

Fig. 17. Force responses in closed loop force control for teleoperation.

The kinematics for position and differential motion is developed for this 6-DOF haptic device. Jacobian and static force analysis is also presented to define the relation between the applied forces and motor torques.

Teleoperation control system of a 6-DOF serial robot using this new 6-DOF haptic device is constructed and realized on the digital controller. The closed loop force control system is designed and analyzed. Error analysis of the closed loop control system shows that undesired dynamic forces caused by haptic device can be reduced by increasing the force controller gain.

The tracking performances of the slave robot and measured user forces and contact forces for the closed loop force control are compared with those for the open loop control. When the open loop force control is applied, some force errors between the applied forces and the contacting forces were produced. These force errors could be significantly reduced when the closed loop force control is applied. The user applied forces of the steering handle could track the contact forces from environment well. However, the closed loop force control is susceptible to noises in control forces because of the control actions and sensor noises. The closed loop control also requires an additional costly force sensor for measuring the user applied force.

Future works for teleoperation using haptic devices are devoted to the dynamic analysis of the 6-DOF parallel haptic device and the stability analysis of the teleoperation control system.

REFERENCES

[1] A. M. Tahmasebi, B. Taati, F. Mobasser, and K. H. Zaad, "Dynamic parameter identification and analysis of a PHANToM haptic device," in *Proc. IEEE Conf. Control Appl.*, Toronto, ON, Canada, Aug. 2005, pp. 1251–1256.

[2] A. J. Silva, O. A. D. Ramırez, V. P. Vega, and J. P. O. Oliver, "PHANToM OMNI haptic device: Kinematic and manipulability," in *Proc. IEEE Conf. Electron., Robot. Automot. Mech.*, 2009, pp. 193–198.

[3] P. Garrec, J. P. Friconneau, and F. Louveau, "VIRTUOSE 6D: A new force control master arm using innovative ball screw actuators," in *Proc. 35th Int. Symp. Robot.*, Paris, France, Mar. 23–26, 2004.

[4] S. D. Laycock and A. M. Day, "Recent developments and applications of haptic devices," *Comput. Graph. Forum*, vol. 22, no. 2, pp. 117–132, Jun. 2003.

[5] J. Martin and J. Savall, "Mechanisms for haptic torque feedback," in *Proc. 1st Conf. Symp. Haptic Interfaces Virtual Environ. Teleoperator Syst.*, San Sebastian, Spain, 2005, pp. 611–614.

[6] J. M. Sabater, R. J. Saltaren, and R. Aracil, "Design, modeling and implementation of a 6URS parallel haptic device," *Robot. Auton. Syst.*, vol. 47, no. 1, pp. 1–10, May 2004.

[7] S. S. Lee and J. M. Lee, "Design of a general purpose 6-DOF haptic interface," *Mechatronics*, vol. 13, no. 7, pp. 697–722, Sep. 2003.

[8] J. Yoon and J. Ryu, "Design, fabrication, and evaluation of a new haptic device using a parallel mechanism," *IEEE/ASME Trans. Mechatronics*, vol. 6, no. 3, pp. 221–233, Sep. 2001.

[9] D. Ryu, J. Song, C. Cho, S. Kang, and M. Kim, "Development of a six DOF haptic master for teleoperation of a mobile manipulator," *Mechatronics*, vol. 20, no. 2, pp. 181–191, Mar. 2010.

[10] C. D. Lee, D. A. Lawrence, and L. Y. Pa, "Isotropic force control for haptic interfaces," *Control Eng. Pract.*, vol. 12, no. 11, pp. 1423–1436, Nov. 2004.

[11] L. J. Stocco and E. Salcudean, "Optimal kinematic design of a haptic pen," *IEEE/ASME Trans. Mechatronics*, vol. 6, no. 3, pp. 210–220, Sep. 2001.

[12] X. He and Y. Chen, "Six-degree-of-freedom haptic rendering in virtual teleoperation," *IEEE Trans. Instrum. Meas.*, vol. 57, no. 9, pp. 1866–1875, Sep. 2008.

[13] M. Orozco and A. El Saddik, "AdHapticA: Adaptive haptic application framework," *IEEE Trans. Instrum. Meas.*, vol. 57, no. 9, pp. 1840–1851, Sep. 2008.
[14] A. El Saddik, M. Orozco, Y. Asfaw, S. Shirmohammadi, and A. Adler, "A novel biometric system for identification and verification of haptic users," *IEEE Trans. Instrum. Meas.*, vol. 56, no. 3, pp. 895–906, Jun. 2007.
[15] G. S. Gupta, S. C. Mukhopadhyay, C. H. Messom, and S. N. Demidenko, "Master-slave control of a teleoperated anthropomorphic robotic arm with gripping force sensing," *IEEE Trans. Instrum. Meas.*, vol. 55, no. 6, pp. 2136–2145, Dec. 2006.
[16] C. Preusche, T. Ortmaier, and G. Hirzinger, "Teleoperation concepts in minimal invasive surgery," *Control Eng. Pract.*, vol. 10, no. 11, pp. 1245–1250, Nov. 2002.
[17] Z. Zhang and D. Zhao, "Master-slave control strategy of telemanipulator," in *Proc. Int. Conf. Robot. Biomimetics*, Guilin, China, 2009, pp. 2063–2067.
[18] K. Vlachos and E. Papadopoulos, "Analysis and experiments of a haptic telemanipulation environment for a microrobot driven by centripetal forces," *J. Comput. Inf. Sci. Eng.*, vol. 8, no. 4, p. 041 007, Dec. 2008.
[19] N. Ando, M. Ohta, and H. Hashimoto, "Micro teleoperation with haptic interface," in *Proc. 26th IEEE IECON*, 2002, vol. 1, pp. 13–18.
[20] A. Frisoli, E. Sotgiu, C. A. Avizzano, D. Checcacci, and M. Bergamasco, "Force-based impedance control of a haptic master system for teleoperation," *Sens. Rev.*, vol. 24, no. 1, pp. 42–50, 2004.
[21] E. L. Faulring, J. E. Colgate, and M. A. Peshkin, "The cobotic hand controller: Design, control and performance of a novel haptic display," *Int. J. Robot. Res.*, vol. 25, no. 11, pp. 1099–1119, 2006.
[22] K. Wen, D. Necsulescu, and J. Sasiadek, "Haptic force control based on impedance/admittance control aided by visual feedback," *Multimedia Tools Appl.*, vol. 37, no. 1, pp. 39–52, Mar. 2008.
[23] J. J. Gil, A. Rubio, and J. Savall, "Decreasing the apparent inertia of an impedance haptic device by using force feedforward," *IEEE Trans. Control Syst. Technol.*, vol. 17, no. 4, pp. 833–838, Jul. 2009.
[24] V. M. Hung and U. J. Na, "Tele-operation of a 6-DOF serial robot using a new 6-DOF haptic interface," in *Proc. IEEE Int. Symp. Haptic Audio-Visual, Environ. Games*, Phoenix, AZ, Oct. 2010, pp. 1–6.
[25] M. A. Laribi, L. Romdhane, and S. Zeghloul, "Analysis and dimensional synthesis of the DELTA robot for a prescribed workspace," *Mechanism Mach. Theory*, vol. 42, no. 7, pp. 859–870, Jul. 2007.

Minh Hung Vu received the B.Sc. degree in automatic control from Hanoi University of Technology, Hanoi, Vietnam, in 2004 and the M.Sc. degree in mechatronics from Asian Institute of Technology, Bangkok, Thailand, in 2007. He is currently working toward the Ph.D. degree with the School of Mechanical engineering and Automation, Kyungnam University, Masan, Korea.

His current research interests include optimal designs, kinematics and dynamic analysis, intelligent control and teleoperation for haptic devices, robots and mechatronic system.

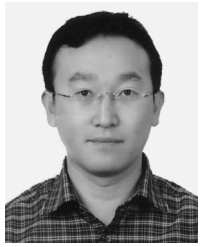

Uhn Joo Na received the Ph.D. degree in mechanical engineering from Texas A&M University, College Station, in 2000.

He was a senior researcher at Korea Institute of Machinery and Material (KIMM) from 2002 to 2004 before joining the faculty at Kyungnam University, Masan, Korea. He is currently an associate professor in the School of Mechanical Engineering and Automation, Kyungnam University. His current research interests include haptic device design and control, teleoperation. human-machine interaction, robotic hand, magnetic bearings.